



Article

Crystal Structure and Magnetic Properties of Trinuclear Transition Metal Complexes (Mn^{II}, Co^{II}, Ni^{II} and Cu^{II}) with Bridging Sulfonate-Functionalized 1,2,4-Triazole Derivatives

Andrea Moneo-Corcuera ^{1,*}, Breogán Pato-Doldan ^{1,†} , Irene Sánchez-Molina ¹, David Nieto-Castro ^{1,2} and José Ramón Galán-Mascarós ^{1,3,*} 

¹ Institute of Chemical Research of Catalonia (ICIQ), The Barcelona Institute of Science and Technology (BIST), Av. Països Catalans, 16, 43007 Tarragona, Spain; breogan.pato@gmail.com (B.P.-D.); isanchez@iciq.es (I.S.-M.); dniето@iciq.es (D.N.-C.)

² Departament de Química Física I Inorgànica, Universitat Rovira I Virgili, C/Marcel·lí Domingo, 43007 Tarragona, Spain

³ ICREA, Passeig Lluís Companys 23, 08010 Barcelona, Spain

* Correspondence: amoneo@iciq.es (A.M.-C.); jrgalan@iciq.es (J.R.G.-M.)

† Insud Farma. Laboratorios León Farma, S.S. C/La Vallina, S/N 24193, Navatejera, León, Spain.



Citation: Moneo-Corcuera, A.; Pato-Doldan, B.; Sánchez-Molina, I.; Nieto-Castro, D.; Galán-Mascarós, J.R. Crystal Structure and Magnetic Properties of Trinuclear Transition Metal Complexes (Mn^{II}, Co^{II}, Ni^{II} and Cu^{II}) with Bridging Sulfonate-Functionalized 1,2,4-Triazole Derivatives. *Molecules* **2021**, *26*, 6020. <https://doi.org/10.3390/molecules26196020>

Academic Editors: Salah Massoud and Febee Louka

Received: 30 August 2021

Accepted: 2 October 2021

Published: 4 October 2021

Publisher's Note: MDPI stays neutral with regard to jurisdictional claims in published maps and institutional affiliations.



Copyright: © 2021 by the authors. Licensee MDPI, Basel, Switzerland. This article is an open access article distributed under the terms and conditions of the Creative Commons Attribution (CC BY) license (<https://creativecommons.org/licenses/by/4.0/>).

Abstract: Here we present the synthesis, structure and magnetic properties of complexes of general formula (Mn)(Me₂NH₂)₄[Mn₃(μ-L)₆(H₂O)₆] and (Me₂NH₂)₆[M₃(μ-L)₆(H₂O)₆] (M = Co^{II}, Ni^{II} and Cu^{II}); L²⁻ = 4-(1,2,4-triazol-4-yl) ethanedisulfonate). The trinuclear polyanions were isolated as dimethylammonium salts, and their crystal structures determined by single crystal and powder X-ray diffraction data. The polyanionic part of these salts have the same molecular structure, which consists of a linear array of metal(II) ions linked by triple N1-N2-triazole bridges. In turn, the composition and crystal packing of the Mn^{II} salt differs from the rest of the complexes (with six dimethyl ammonia as counteranions) in containing one Mn²⁺ and four dimethyl ammonia as counteranions. Magnetic data indicate dominant intramolecular antiferromagnetic interactions stabilizing a paramagnetic ground state. Susceptibility data have been successfully modeled with a simple isotropic Hamiltonian for a centrosymmetric linear trimer, $H = -2J(S_1S_2 + S_2S_3)$ with super-exchange parameters $J = -0.4$ K for Mn^{II}, -7.5 K for Ni^{II} and -45 K for Cu^{II} complex. The magnetic properties of these complexes and their easy processing opens unique possibilities for their incorporation as magnetic molecular probes into such hybrid materials as magnetic/conducting multifunctional materials or as dopant for organic conducting polymers.

Keywords: linear trimers; crystal structure; magnetic exchange; coordination chemistry

1. Introduction

Molecule-based magnetism has attracted the attention of a great number of researchers due to its multidisciplinary and its applications in such fields as (nano)electronics [1–3], quantum computing [4], spintronics [5,6] and molecular biology [7,8]. From a more fundamental point of view, molecular magnetism aims at offering a profound comprehension of magneto-structural correlations of molecular magnetic materials. Coordination chemistry appears as a powerful tool to design novel materials with tailor-made magnetic properties [9–13].

In this context, polymetallic complexes are ideal compounds for studying magnetic and electronic interactions between magnetic metal centers in a controlled (molecular) environment. In particular, the investigation of spin coupling effects over long distances has been of high interest for metalloprotein studies [14] and engineering of molecule-based spintronic devices [15]. Exchange spin coupling, or superexchange, is a phenomenon in molecular magnetic systems. The study of magnetic interactions between ions through

non-magnetic connecting atoms (linkers) is a challenging task in extended solids [16,17], whereas molecules offer a controlled and tunable framework where spin carriers and linkers can be incorporated as building blocks in the desired connectivity, allowing for analysis based on their localized/molecular nature.

The chemical design and synthesis of bridging ligands, which provides effective pathways to transmit spin coupling effects, promotes an attractive strategy for creating novel and interesting polynuclear complexes with desirable magnetic properties. In particular, 1,2,4-triazole and its derivatives, due to their capacity to form N₁-N₂ bridges between metal centers, are interesting ligands for forming stable coordination structures of different dimensionalities, such as discrete polynuclear metal complexes [18–21], 1D/2D polymers [22–26] or 3D metal–organic frameworks (MOFs) [27–31]. The N₁-N₂-1,2,4-triazole bridges offer short and conjugated diatomic pathways to propagate an effective superexchange between the paramagnetic metal centers. Moreover, the nitrogen donor atoms of the triazole ring can create a suitable ligand field for spin transition in ferrous complexes [32–34], which provides a potential approach to molecule-based data storage application [35–37].

All these reasons justify the use of discrete polynuclear complexes from derived 1,2,4-triazoles in the study of magnetic interactions between metal centers. In recent years, a large number of polynuclear compounds based on 1,2,4-triazole and its derivatives have been synthesized and investigated to further understand magnetic superexchange coupling [38–40].

The chemical nature of the triazole substituents influence the structure and magnetic properties of their complexes [28–40]. Among the family of 1,2,4-triazoles, the 4-functionalized derivatives have been the most studied for the development of magnetic materials. This type of functionalization does not sterically hinder the N₁-N₂ bridging coordination mode, and the functional group might additionally offer different structural motifs to the coordination complexes. In the literature, the most common functional groups in this 4-position are aromatic rings/heterocycles, including pyridyls [41–43], triazol [44,45] or tetrazoles [46], and alkyl tails [47]. All of them lead to the formation of neutral ligands, and therefore to the synthesis of cationic coordination metal complexes. Among them, a large variety of triazol-based Fe^{II} systems, including [Fe(4-*R*-1,2,4-triazole)₃]²⁺ polymers and discrete polynuclear complexes, reveal spin crossover (SCO) behaviour [48–51].

Recently, our group synthesized a dianionic triazole ligand (L²⁻ = 4-(1,2,4-triazol-4-yl)ethanedisulfonate) with two sulfonated groups in the functional moieties at the 4-position of the triazol. The polar and anionic nature of this ligand would increase solubility and stability in polar solvents of the resulting coordination complexes, facilitating their posterior processing into magnetic hybrid materials. The coordination of this dianionic ligand with iron (II) ions led to the formation of a polyanionic Fe^{II} trinuclear complex with a spin transition above room temperature [52]. Here we present the synthesis, crystal structure and magnetic properties of first-row transition metal complexes (Mn^{II}, Co^{II}, Ni^{II} and Cu^{II}) with this anionic ligand (L), in order to investigate the structure and magnetic behavior of these polyanionic trimers, establishing a rational magneto-structural correlation.

2. Results

2.1. Synthesis of the Complexes

The complexes were synthesized by reacting the ligand, (Me₂NH₂)₆L (Dimethylammonium 4-(1,2,4-triazol-4-yl)ethanedisulfonate), and the corresponding perchlorate metal salt in water in a 2.5:1 molar ratio, leading to the formation of polyanionic linear trinuclear complexes with the formula [M₃(μ-L)₆(H₂O)₆]^{−6} [M = Mn^{II} (**Mn**), Co^{II} (**Co**), Ni^{II} (**Ni**), or Cu^{II} (**Cu**)]. These complexes were isolated in solid state as the corresponding dimethyl ammonium salts by slow ethanol vapor diffusion into the aqueous reaction mixture (Figure S1a). This crystallization process yielded needle-shaped crystals for **Mn**, **Co** and **Ni**, with distinct colors depending on the metal: colorless for Mn^{II}, orange for Co^{II}, and blue-purple for Ni^{II} (Figure S1b). The high quality of these crystals enabled us to determine their crystal structure from single crystal X-Ray diffraction data. We could not

isolate Cu complex as single crystals, although highly crystalline powder was obtained, and their crystal lattice was determined by Pawley fit of the X-Ray powder diffractogram.

2.2. Structural Characterization

The structure of **Mn**, **Co** and **Ni** was elucidated from single crystal X-Ray diffraction data, collected at 100 K. Crystallographic refinement showed that the three compounds contain the same polyanionic trinuclear units, crystallizing in the triclinic $P\bar{1}$ space group (see detailed crystallographic data in Table S1). All of them contain analogous metallic complexes formed by a linear array of three transition metal centers connected by six triazole ligands via two triple N₁-N₂ bridges (Figure 1a). These complexes show structure similar to that observed in analogous trinuclear metal complexes based on 4(*R*)-1,2,4-triazole [19]. Thus, the central metal cation is in a MN₆ octahedral configuration, whereas the terminal metal cations show an MN₃O₃ *fac*-octahedral configuration with three nitrogen atoms from the bridging triazole ligands and three oxygen atoms from water molecules occupying the terminal coordination positions. This yields a polyanion with a total charge of -6 , given their $(M_3^{+2}L_6^{-2}) \cdot (H_2O)_6$ composition. Geometry parameters for these trimers in each compound are summarized in Figure S2 and Table S2. The metal-ligand bonding distances indicate high spin (HS) configurations for all metal positions (average M-N (Å) = 2.239, 2.121 and 2.064 for **Mn**, **Co** and **Ni**, respectively), in good agreement with the corresponding metal ion radii in HS state [$r(Mn^{II}_{HS}) = 97$ pm, $r(Co^{II}_{HS}) = 88$ pm and $r(Ni^{II}_{HS}) = 83$ pm] [52,53].

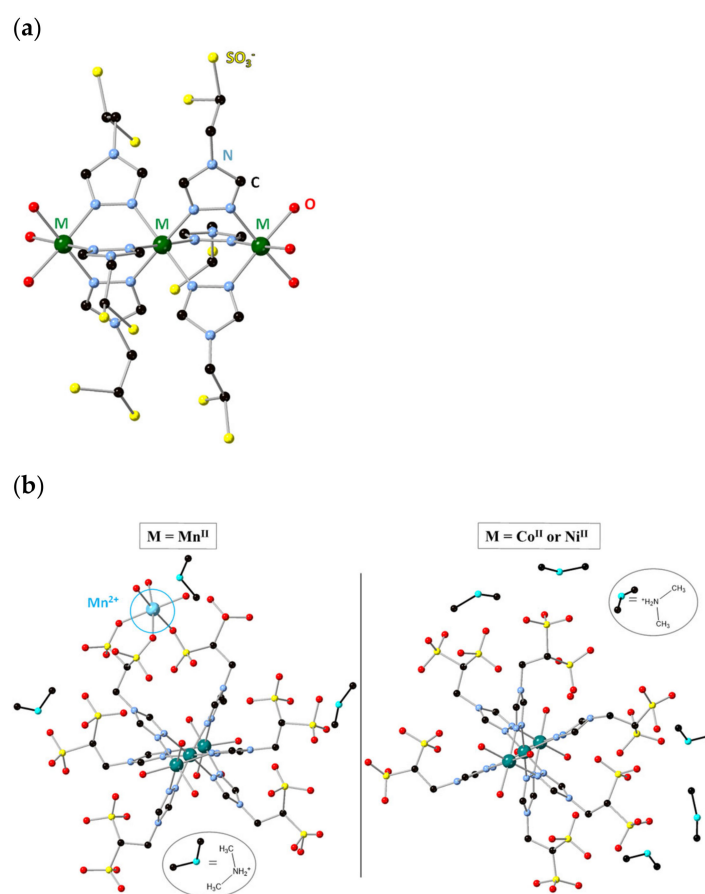


Figure 1. (a) Chemical structure of the polyanionic part for all the complexes. Oxygen atoms from the sulfonated groups were omitted for clarity. (b) Representation of the anionic part with counteranions. Hydrogen atoms are omitted for clarity. Dimethyl ammonium cations (disordered) are represented only in one of their crystallographic positions.

Although all single crystals confirmed the presence of analogous trimers, the packing is slightly different for **Mn**; whereas **Co** and **Ni** complexes are isostructural with consistent cell parameters and analogous unit cell contents (Table S1), the anionic Mn^{II} trimer crystallizes with a slightly different counter ion content, formed by one Mn^{II} and four $[(\text{CH}_3)_2\text{NH}_2]^+$ moieties. The Mn^{2+} cation external to the trimer occupies a nearby crystallographic position, directly coordinated to three sulfonate groups and completing its coordination geometry with three interstitial water molecules (Figure 1b).

Regarding the crystallographic packing, the trimers are oriented parallel to the z axis, forming chains via inter-trimer H-bonds between coordinated water molecules and sulfonated groups (Figure S3). These chains of trimers are also connected to each other along the x and y axis by additional intermolecular H-bonding interactions [$d(\text{O}\cdots\text{H}) = 1.9\text{--}2.3$ Å for **Mn**; $d(\text{O}\cdots\text{H}) = 1.9\text{--}2.1$ Å for **Co** and **Ni**]. Dimethyl ammonium cations and water molecules are disordered in the interstices of this anionic network.

In order to confirm the phase purity of these compounds in bulk, we analyzed the powder X-ray diffraction (PXRD) data of the polycrystalline samples. Pawley fits were carried out on the experimental diffractograms (Figure S4), obtaining refined cell parameters for each sample (Table S3). The refined cell parameters for **Mn**, **Co** and **Ni** are in good agreement with single crystal data, confirming a single crystallographic phase. The PXRD data for **Cu** was successfully reproduced with a Pawley fitting confirming that this material is isostructural to the Co^{II} and Ni^{II} salts, with consistent cell parameters (Table S3). This is also supported by IR spectroscopy, which shows identical spectra for all the complexes (Figure S5).

2.3. Magnetic Measurements

Magnetic susceptibility (χ_m) measurements for all the compounds were performed in the 300–2 K range, with an applied magnetic field of 0.1 T (Figure 2). The $\chi_m T$ products of **Mn**, **Co** and **Ni** at room temperature were in good agreement with the expected values for magnetically diluted high spin samples with $g \approx 2$ (Table 1). As expected, the Co^{II} trimer exhibited larger $\chi_m T$ values as a result of its high magnetic anisotropy ($g > 2$), typically found in octahedral Co^{II} ions [54].

Below a certain temperature, the $\chi_m T$ value starts to decrease, suggesting the presence of antiferromagnetic (AF) intramolecular interactions. In good agreement, negative Weiss constants (θ) were obtained by fitting the experimental magnetic data (>50 K) to a Curie–Weiss Law (Equations (S1) and (S2), Figure S6 and Table 1).

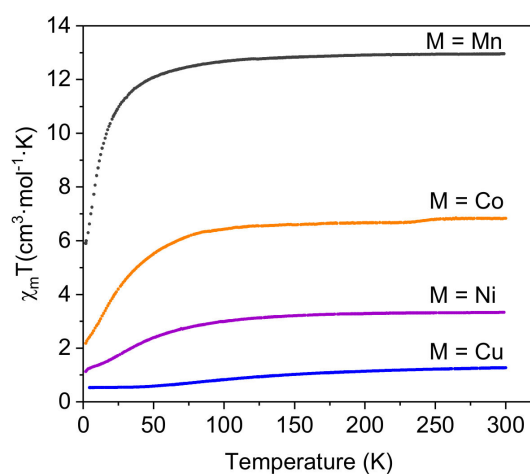


Figure 2. Magnetic susceptibility data for $[\text{M}_3(\mu\text{-L})_6(\text{H}_2\text{O})_6]^{-6}$ complexes within 300–2 K range.

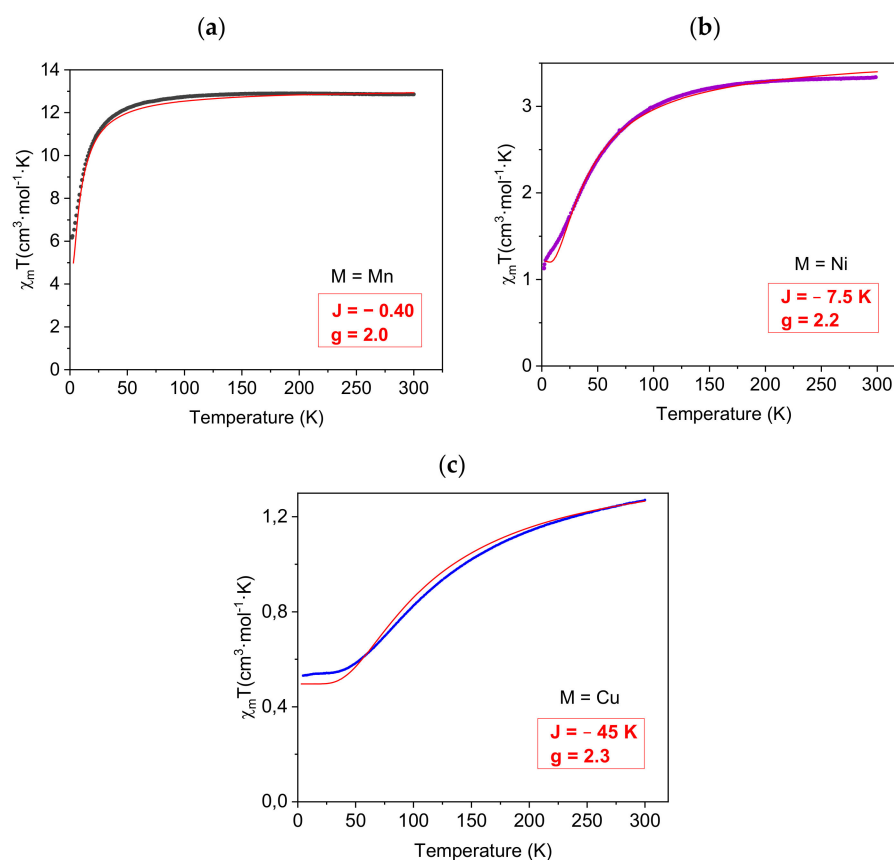
Table 1. Comparison of theoretical and experimental $\chi_m T$ product and Curie–Weiss parameters (C and θ) for all the complexes.

| Complex | $\chi_m T_{\text{theoretical}}$ ($\text{cm}^3 \cdot \text{mol}^{-1} \cdot \text{K}$) | $\chi_m T_{\text{experimental}}$ ($\text{cm}^3 \cdot \text{mol}^{-1} \cdot \text{K}$) | C ($\text{cm}^3 \cdot \text{mol}^{-1} \cdot \text{K}$) | θ (K) |
|-----------|---|--|---|-----------------|
| Mn | 13.12 | 12.95 | 13.13 | −3.76 |
| Co | 5.60 | 6.82 | 7.07 | −11.26 |
| Ni | 3.00 | 3.32 | 3.59 | −20.25 |
| Cu | 1.20 | 1.26 | 1.74 | −108.48 |

In order to quantify the intra-trimer spin–spin coupling, the magnetic susceptibility data for **Mn**, **Ni** and **Cu** were modelled, as a first approximation, to a centro-symmetrical linear trimer (Figure S7) by using the isotropic Hamiltonian (Equation (1)):

$$H = 2J s_2 (s_1 + s_3) \quad (1)$$

where s_n are the spins of the different metal centers and J is the corresponding superexchange constant. In a first approximation, intermolecular interactions and zero field splitting contributions are considered to be negligible. The couplings between terminal metal centers are also omitted due to the long metal-to-metal distances ($\approx 7.5 \text{ \AA}$) and the inefficient pathway for magnetic exchange between them [55]. Based on this isotropic model, the susceptibility data were successfully reproduced with the MAGPACK package [56,57], obtaining the best fit parameters (J and g) for **Mn**, **Ni** and **Cu** (Figure 3). The magnetic behavior for **Co** could not be modelled with this approximation, and will be discussed later.

**Figure 3.** Plots of $\chi_m T$ vs. T for **Mn** (a), **Ni** (b) and **Cu** (c), and their corresponding best-fit curves (red line) obtained with the MAGPACK package.

In the Mn^{II} compound (Figure 3a), the $\chi_{\text{m}}T$ product at 300 K is $12.94 \text{ cm}^3 \cdot \text{mol}^{-1} \cdot \text{K}$, in agreement with the presence of three high spin Mn^{II} ions with $S = 5/2$. This value remains constant down to 70 K. At lower temperatures, the $\chi_{\text{m}}T$ product decreases rapidly to reach $5.90 \text{ cm}^3 \cdot \text{mol}^{-1} \cdot \text{K}$ at 2 K. This behavior was successfully modelled for the isotropic trinuclear model with best fitting parameters $g = 2.0$ and $J = -0.4 \text{ K}$, which is in good agreement with J values previously reported for triazole-bridged Mn^{II} centers [58,59].

The Ni^{II} compound data (Figure 3b) reveals a $\chi_{\text{m}}T$ value of $3.33 \text{ cm}^3 \cdot \text{mol}^{-1} \cdot \text{K}$ at 300 K, which is consistent with the presence of three high spin Ni^{II} ions with $S = 1$. $\chi_{\text{m}}T$ remains constant down to 150 K, when it starts to decrease quickly down to $1.12 \text{ cm}^3 \cdot \text{mol}^{-1} \cdot \text{K}$ at 2 K. The best fitting of these experimental data with the isotropic trimer model yielded $g = 2.2$ and $J = -7.5 \text{ K}$, again in good agreement triazole-bridged Ni^{II} centers (J from -13.8 to -6.7 K) [60–62].

In the Cu^{II} complex (Figure 3c), the $\chi_{\text{m}}T$ product at 300 K is $1.27 \text{ cm}^3 \cdot \text{mol}^{-1} \cdot \text{K}$, which corresponds to the spin-only value for three Cu^{II} ions $S = 1/2$. Upon being subjected to the cooling process, $\chi_{\text{m}}T$ decreases gradually to reach a constant value around $0.53 \text{ cm}^3 \cdot \text{mol}^{-1} \cdot \text{K}$ below 15 K. This experimental data can be well-modelled with $J = -45 \text{ K}$ and $g = 2.3$. The value of J parameter is in good agreement with previous reported values for triazole-bridged Cu^{II} centers, where magnetic superexchange only occurs through the N-N bridge that lies in equatorial position with respect to the magnetic $d_{x^2-y^2}$ orbital (Figure 4) [63]. The equatorial configuration of the triazol ensures a good orbital overlap, enhancing the efficient metal-to-metal magnetic interactions [64–66]. Consequently, our J value represents weaker antiferromagnetic interaction when compared with the J values between -70 K [67] and -107 K [63] found in analogue Cu^{II} complexes where the bridging modes favor better orbital overlap.

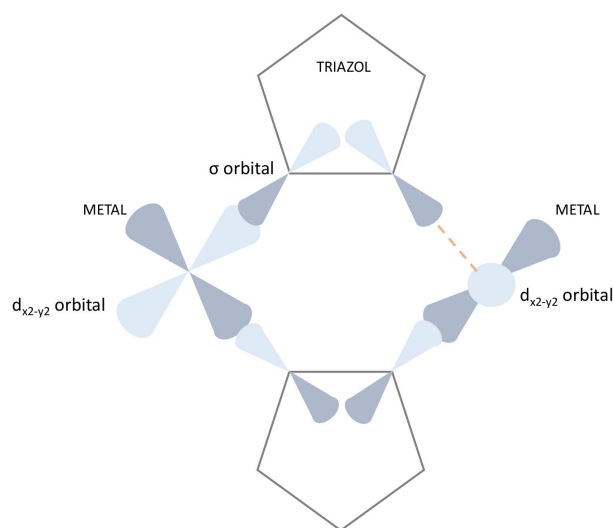


Figure 4. Schematic representation of magnetic molecular orbitals in triazole-bridged complexes. The bridge in the bottom represents the σ overlap for an efficient AF exchange propagation. The bridge in the top represents an absence of orbital overlapping (dotted orange line).

The Co^{II} compound cannot be appropriately modeled with the isotropic model used due to the spin orbit coupling and high single-ion anisotropy [68–70]. In the literature, some linear Co^{II} trinuclear complexes with triazole ligands have been modeled with modified Lines approximations [60], showing J value between -6.9 K [55] and -4 K [62].

Field-dependence of the magnetization (M) was also measured at 2 K (Figure 5). The experimental curves are fitted with MAGPACK by using J and g parameters obtained from susceptibility data. The M vs. H curves for all the complexes show a similar field dependence. At low applied fields, the magnetization is proportionally linear to the magnetic field, effectively described by the Curie Law. When the magnetic field becomes larger, the magnetization tends to a saturation value, M_s (generally described as Equation (S3)).

The saturation values for **Co**, **Ni** and **Cu** are in good agreement with an antiferromagnetic ground state (Table 2). In the case of **Mn**, this initial saturation limit is broken above ≈ 4 T, appearing as a second increase that continues monotonically up to the maximum applied field (7 T) without any sign of reaching a new saturation value.

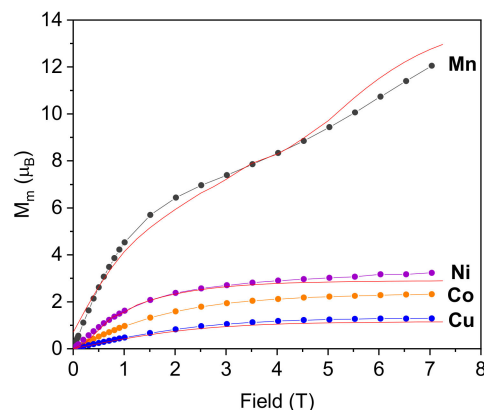


Figure 5. Magnetization (M) vs. magnetic field (H) plots at 2 K for $[M_3(\mu-L)_6(H_2O)_6]^{-6}$ complexes and their corresponding fit curves (red line) obtained with the MAGPACK package, with the resulting parameters of XT vs. T best-fitting.

Table 2. Comparison of experimental and theoretical saturation magnetization for the antiferromagnetically (AF) coupled ground state with $g = 2$ for all the complexes.

| Complex | M_s (AF) (μ_B) | M_s (experimental) (μ_B) |
|-----------|---------------------------|-------------------------------------|
| Mn | 5.00 | 12.05 |
| Co | 4.00 | 3.22 |
| Ni | 3.00 | 2.32 |
| Cu | 1.00 | 1.29 |

These results can be rationalized by taking into account the energy levels of the electronic states (Equation (S4), Table S4 and Figure S8). Accordingly, **Mn** exhibits the lowest energy difference between the ground AF state and the excited states. Thus, the applied magnetic field facilitates the population of excited states due to Zeeman splitting, breaking the saturation limit expected for the AF ground state. Even at 7 T, the M_s is far from the maximum ferromagnetic alignment. In the rest of the series the magnetic fields applied are not strong enough to provoke the same effect since all samples reach saturation at relatively low applied fields.

3. Materials and Methods

3.1. Materials and Physical Measurements

All reagents were used as purchased without further purification. Inductively coupled plasma optical emission spectrometry (ICP-OES) analytical data was obtained with an Agilent 755-ES (Santa Clara, CA, USA inductively coupled plasma optical emission spectrometer at the University of Valladolid. Infrared spectroscopy (IR) data were collected with an FTIR Bruker spectrometer (Billerica, MA, USA) model Alpha equipped with an ATR accessory. X-Ray powder diffraction (XRPD) data was collected with a Siemens D5000 diffractometer (Bragg–Brentano parafocusing geometry and vertical θ – θ goniometer, Berlin, Germany) fitted with a curved graphite diffracted-beam monochromator, incident and diffracted-beam Soller slits, a 0.06° receiving slit, and a scintillation counter as a detector. The angular 2θ diffraction range was between 5° and 40° . Data were collected with an angular step of 0.05° at 10 s per step and sample rotation. A low background Si(510) wafer was used as a sample holder. Cu $K\alpha$ radiation was obtained from a copper X-ray

tube operated at 40 kV and 30 mA. The obtained XRPD patterns were analyzed by Pawley profile analysis (between 8° and 35°) using the TOPAS software [71]. A Chebyshev function of seven terms was used to fit the background. Magnetic measurements were carried out on fine-grained powders with a Quantum Design MPMS-XL SQUID magnetometer (Quantum Design, Inc., San Diego, CA, USA). Variable temperature magnetic susceptibility measurements were carried out under an applied field of 1000 Oe at 1 K·min⁻¹ between 300 and 2 K. Variable field magnetization measurements were carried out at 2 K from 0 to 7 T.

3.2. Synthesis of the Ligand (L)

(Me₂NH₂)₂L (Dimethyl-ammonium 4-(1,2,4-triazol-4-yl)ethanedisulfonate 4-(1,2,4-triazol-4-yl)ethanedisulfonate) was synthesized as previously reported [53].

3.3. Synthesis of the Complexes (Mn, Ni and Cu)

(Me₂NH₂)₆[M₃(μ-L)₆(H₂O)₆]-M = Co^{II} (**Co**), Ni^{II} (**Ni**) and Cu^{II} (**Cu**)- and (Mn)(Me₂NH₂)₄[[Mn₃(μ-L)₆(H₂O)₆] (**Mn**) were synthesized by dissolving M(ClO₄)₂·6H₂O (0.05 mmol) and (Me₂NH₂)₆L (0.05 g; 0.14 mmol) in water and then mixed (total volume 2 mL). Crystals of Mn^{II}, Co^{II} and Ni^{II} complexes and crystalline powder of Cu^{II} complex were isolated by slow ethanol vapor diffusion.

Mn: IR (ATR): ν = 3420, 3114, 1632, 1205, 1020, 838, 716, 636, 592, 505. ICP experimental and calculated for C₃₂H₉₃Mn₄N₂₂O₅₃S₁₂ (2238.72 g/mol) (%_{exp}; %_{calc}): C (16.99%; 17.16%), H (3.91%; 4.18%), N (14.27%; 13.76%), S (17.31%; 17.18%).

Co: IR (ATR): ν = 3420, 3114, 1632, 1205, 1020, 838, 716, 636, 592, 505. Elemental Analysis experimental and calculated for C₃₆H₁₀₂Co₃N₂₄O₄₈S₁₂ (2200.90 g/mol) (%_{exp}; %_{calc}): C (18.28%; 19.06%), H (4.04%; 4.67%), N (14.10%; 15.27%), S (16.51%; 17.48%).

Ni: IR (ATR): ν = 3420, 3121, 1653, 1204, 1020, 844, 715, 639, 595, 505. Elemental Analysis experimental and calculated for C₃₆H₁₀₀Ni₃N₂₄O₄₇S₁₂ (2182.17 g/mol) (%_{exp}; %_{calc}): C (16.08%; 17.06%), H (4.09%; 4.61%), N (15.42%; 15.40%), S (16.14%; 17.63%).

Cu: IR (ATR): ν = 3467, 3119, 1643, 1205, 1020, 837, 712, 639, 589, 510. Elemental Analysis experimental and calculated for C₃₆H₁₀₀N₂₄Cu₃O₄₇S₁₂ (2196.73 g/mol) (%_{exp}; %_{calc}): C (19.30%; 19.68%), H (4.61%; 4.58%), N (15.53%; 15.30%), S (16.61%; 17.51%).

3.4. Single Crystal X-ray Diffraction

Data were collected at 100(2) K on a Bruker-Nonius diffractometer (Billerica, MA, USA) with an APPEX 2 4K CCD area detector using Mo-Kα (λ = 0.71073 Å) and equipped with an Oxford Cryostem 700 plus. Crystal structure solution was obtained using SIR2011 and refinement was performed using SHELXL v. 2018/3 under the ShelXle (Rev. 912) interface. All non-hydrogen atoms were refined anisotropically.

The complexes contain a trinuclear polyanion [M₃(μ-L)₆(H₂O)₆]⁶⁻, formed by a linear array of octahedral metal(II) ions (M1-M2-M1) connected by two triple μ-triazole bridges (Figure S2). The central metal positions have a MN₆ configuration and the terminal metal position completes its N₃O₃ hexacoordination with three H₂O molecules in fac conformation. The asymmetric unit of **Mn** contains one molecule of the Mn^{II} trimer coordinated by six water molecules, four dimethyl ammonium cations, 8.25 non-coordinated water molecules and one manganese cation (+2). This latter is bonded to three water molecules and three sulfonate groups. Most of the sulfonate rests are disordered in different orientations. The dimethylammonium cations are disordered in 11 positions with different occupancies summing a total of four cations. The non-coordinated water molecules are disordered in 14 positions with different occupancies. The asymmetric unit of **Co** and **Ni** contains one molecule of the trinuclear metal complex, six dimethyl ammonium cations and 6.25 and 4.90 water molecules, respectively. Most of the sulfonate rests on the main molecule are disordered in two orientations. The dimethylammonium cations are disordered in 15 positions with different occupancies summing a total of six cations. The non-coordinated water molecules are disordered in 21 and 13 positions with different

occupancies. Although the unit cells of these structures are quite similar to **Mn**, they are not isostructural and the gamma angle of the triclinic cell differs from $83.8^\circ/83.6^\circ$ at **Co/Ni** to 87.4° at **Mn**. The structures of **Co** and **Ni** were refined with strong damping factors based on the isostructural iron derivative (CCDC 1016539); after some corrections and omitting the damping factors, refinement remained consistent. The location of the cations and water molecules were extremely diffuse and their positions could only be located using the positions from the iron complex, which offered a much better dataset. Crystallographic data and main refinement parameters are included in Table S1. Crystallographic data for **Mn**, **Co** and **Ni** have been deposited at the Cambridge Crystallographic Database Centre, with deposition numbers CCDC 2045018–2045020, respectively. Copies of this data can be obtained free of charge on application to the CCDC, Cambridge, UK via www.ccdc.cam.ac.uk/data_request/cif.

4. Conclusions

A series of complexes based on polyanionic linear trimers, $[M_3(\mu-L)_6(H_2O)_6]^{-6}$ ($M = Mn^{II}, Co^{II}, Ni^{II}$ and Cu^{II}) have been selectively synthesized via the reaction of the ligand $L^{-2} = 4-(1,2,4\text{-triazol-4-yl})\text{ethanedisulfonate}$ with the corresponding metal(II) perchlorate salts in a 2.5:1 molar ratio. Crystallographic data confirm identical molecular structure for the polyanionic part of all the complexes, formed by three metal ions linked by triply N-N-triazole bridges. The anionic Co^{II}, Ni^{II} and Cu^{II} trimers crystallize with six $[(CH_3)_2NH_2]^+$ moieties, whereas the Mn^{II} complex shows a slightly different counter ion content, formed by one Mn^{II} and four $[(CH_3)_2NH_2]^+$ moieties. Magnetic susceptibility studies showed dominant intra-trimer antiferromagnetic interactions between terminal and central metal positions, as expected for a N_1, N_2 -triazole-bridging mode. An isotropic model for centrosymmetric linear trimers was good enough to model the thermal dependence of the magnetic susceptibility, extracting consistent coupling parameters (J) with the exception of the Co^{II} derivative, considering intermolecular interactions as negligible. The analysis of the magnetization data at very low temperatures and up to 7 T revealed that the ground antiferromagnetic (AF) state is a good descriptor for these trimers with the exception of the Mn^{II} derivative, where excited states with different multiplicity are close enough in energy to become populated by magnetic fields. Regarding the practical utilization of these complexes, the polyanionic nature of these trimers, along with their high solubility and stability in polar solvents, open interesting possibilities for their incorporation into hybrid materials as magnetic components, such as in magnetic/conducting hybrid salts [72] or as doping elements in organic conducting polymers [73]. These studies are under development.

Supplementary Materials: The following are available online. Table S1. Crystallographic data of **Mn**, **Co** and **Ni** crystals; Table S2. Metal-Nitrogen Bond Length for $[M_3(\mu-L)_6(H_2O)_6]^{-6}$ complexes (Figure S2); Table S3. Cell parameters and cell volume obtained from Pawley fit of experimental XRPD pattern shown in Figure S3; Table S4. Energy levels for trimers of **Mn**, **Ni** and **Cu** according to Equation (S4); Figure S1. (a) Pictures of the formation of all the complexes in the synthesis solution after seven days in ethanol vapor flow. (b) Optical microscopic images of **Mn**, **Co** and **Ni** single crystals in their mother liquor; Figure S2. Labeling scheme for the general framework of the $[M_3(\mu-L)_6(H_2O)_6]^{-6}$ complexes. H atoms of coordinating molecules have been omitted for clarity; Figure S3. Packing diagrams showing the arrangement of the trimers. Intratrimer H-bonded interactions ($d(O\cdots H) = 1.9\text{--}2.3/2.1 \text{ \AA}$) are represented by red dotted lines for **Mn/Co** or **Ni**; Figure S4. Pawley fits of the X-ray powder diffraction patterns of the $[M_3(\mu-L)_6(H_2O)_6]^{-6}$ complexes. The experimental and calculated data are represented as red circles and a black solid line respectively, whereas the green line is the difference between them; Figure S5. Infrared spectra for MII complexes. The $400\text{--}700 \text{ cm}^{-1}$ region of the IR spectra is attributed to the metal–ligand stretching vibrations (M-N and M-O vibration modes). The band at 1200 cm^{-1} and 1650 cm^{-1} can be assigned to S=O and C=N stretching, respectively. The bands at 3491 cm^{-1} (OH stretching) and at 1630 cm^{-1} (H-OH bending) evidence the presence of coordinated water molecules; Figure S6. χ^{-1} vs. T plots (solid lines) and their corresponding linear fitting above 50 K (dash lines) for all the complexes; Figure S7.

Centrosymmetrical model of linear trinuclear complexes; Figure S8. Energy Diagram for Mn^{II}, Ni^{II} and Cu^{II} trimers (see Table S4) with those *J* values determined from experimental χT vs. *T* data.

Author Contributions: Conceptualization and paper writing, J.R.G.-M. and A.M.-C.; writing—original draft preparation, J.R.G.-M. and A.M.-C. Experiment design J.R.G.-M., A.M.-C. Investigation, A.M.-C.; Crystal structures, B.P.-D. and A.M.-C. Magnetic measurements A.M.-C., I.S.-M., D.N.-C. All authors have participated in the experiments. All authors have read and agreed to the published version of the manuscript.

Funding: This research was funded by the European Union (ERC StG grant CHEMCOMP no 279313); the Ministerio de Ciencia e Innovación through Severo Ochoa Excellence Accreditation 2020–2023 (CEX2019-000925-S, MIC/AEI); the FEDER/Ministerio de Ciencia e Innovación, Agencia Estatal de Investigación (project RTI2018-095618-B-I00); the Generalitat de Catalunya (2017-SGR-1406), and the CERCA Programme/Generalitat de Catalunya.

Institutional Review Board Statement: Not applicable.

Informed Consent Statement: Not applicable.

Data Availability Statement: Not applicable.

Acknowledgments: Thanks MINECO for a pre/postdoctoral F.P.I. fellowship.

Conflicts of Interest: The authors declare no conflict of interest.

Sample Availability: Samples of the compounds are not available from the authors.

References

1. Verdaguer, M. Molecular electronics emerges from molecular magnetism. *Science* **1996**, *272*, 698–699. [[CrossRef](#)]
2. Joachim, C.; Gimzewski, J.K.; Aviram, A. Electronics using hybrid-molecular and mono-molecular devices. *Nature* **2000**, *408*, 541–548. [[CrossRef](#)]
3. Park, J.; Pasupathy, A.N.; Goldsmith, J.I.; Chang, C.; Yaish, Y.; Petta, J.R.; Rinkoski, M.; Sethna, J.P.; Abruña, H.D.; McEuen, P.L.; et al. Coulomb blockade and the Kondo effect in single-atom transistors. *Nature* **2002**, *417*, 722–725. [[CrossRef](#)]
4. Lehmann, J.; Gaita-Ariño, A.; Coronado, E.; Loss, D. Quantum computing with molecular spin systems. *J. Mater. Chem.* **2009**, *19*, 1672–1677. [[CrossRef](#)]
5. Sanvito, S. Molecular spintronics. *Chem. Soc. Rev.* **2011**, *40*, 3336–3355. [[CrossRef](#)]
6. Chen, J.; Reed, M.A.; Rawlett, A.M.; Tour, J.M. Large on-off ratios and negative differential resistance in a molecular electronic device. *Science* **1999**, *286*, 1550–1552. [[CrossRef](#)] [[PubMed](#)]
7. Chachiyo, T.; Rodriguez, J.H. Structure, electronic configuration, and Mössbauer spectral parameters of an antiferromagnetic Fe₂-peroxo intermediate of methane monooxygenase. *Dalton Trans.* **2012**, *41*, 995–1003. [[CrossRef](#)] [[PubMed](#)]
8. Engelmann, X.; Monte-Pérez, I.; Ray, K. Oxidation Reactions with Bioinspired Mononuclear Non-Heme Metal–Oxo Complexes. *Angew. Chem. Int. Ed.* **2016**, *55*, 7632–7649. [[CrossRef](#)]
9. Ruiz, E.; Rodríguez-Forteza, A.; Alvarez, S. Tailor-made strong exchange magnetic coupling through very long bridging ligands: Theoretical predictions. *Inorg. Chem.* **2003**, *42*, 4881–4884. [[CrossRef](#)] [[PubMed](#)]
10. Pardo, E.; Ruiz-García, R.; Lloret, F.; Faus, J.; Julve, M.; Journaux, Y.; Novak, M.A.; Delgado, F.S.; Ruiz-Pérez, C. Ligand Design for Heterobimetallic Single-Chain Magnets: Synthesis, Crystal Structures, and Magnetic Properties of M₂CuII (M=Mn, Co) Chains with Sterically Hindered Methyl-Substituted Phenylloxamate Bridging Ligand. *Chem. A Eur. J.* **2007**, *13*, 2054–2066. [[CrossRef](#)]
11. Ouellette, W.; Prosvirin, A.V.; Whitenack, K.; Dunbar, K.R.; Zubieta, J. A Thermally and Hydrolytically Stable Microporous Framework Exhibiting Single-Chain Magnetism: Structure and Properties of [Co₂(H_{0.67}bdtd)₃]₂₀ H₂O. *Angew. Chem. Int. Ed.* **2009**, *48*, 2140–2143. [[CrossRef](#)]
12. Galán-Mascarós, J.R.; Coronado, E.; Goddard, P.A.; Singleton, J.; Coldea, A.I.; Wallis, J.D.; Coles, S.J.; Alberola, A. A chiral ferromagnetic molecular metal. *J. Am. Chem. Soc.* **2010**, *132*, 9271–9273. [[CrossRef](#)]
13. Wu, D.Q.; Shao, D.; Wei, X.Q.; Shen, F.X.; Shi, L.; Kempe, D.; Zhang, Y.Z.; Dunbar, K.R.; Wang, X.Y. Reversible On–Off Switching of a Single-Molecule Magnet via a Crystal-to-Crystal Chemical Transformation. *J. Am. Chem. Soc.* **2017**, *139*, 11714–11717. [[CrossRef](#)]
14. Vella, F. The IUBMB and biochemical education. *Biochem. Educ.* **1995**, *23*, 115. [[CrossRef](#)]
15. Coronado, E. Molecular magnetism: From chemical design to spin control in molecules, materials and devices. *Nat. Rev. Mater.* **2020**, *5*, 87–104. [[CrossRef](#)]
16. Kramers, H.A. L'interaction entre les atomes magnétogènes dans un cristal paramagnétique. *Physica* **1934**, *1*, 182–192. [[CrossRef](#)]
17. Anderson, P.W. Antiferromagnetism. *Theory of Superexchange Interaction Phys. Rev.* **1950**, *79*, 350. [[CrossRef](#)]
18. Shakirova, O.G.; Lavrenova, L.G.; Shvedenkov, Y.G.; Berezovskii, G.A.; Naumov, D.Y.; Sheludyakova, L.A.; Dolgushin, G.V.; Larionov, S.V. Synthesis and physicochemical study of iron (II), cobalt (II), nickel (II), and copper (II) complexes with 4-(2-pyridyl)-1, 2, 4-triazole. *Russ. J. Coord. Chem.* **2004**, *30*, 473–479. [[CrossRef](#)]

19. Hogue, R.W.; Singh, S.; Brooker, S. Spin crossover in discrete polynuclear iron (II) complexes. *Chem. Soc. Rev.* **2018**, *47*, 7303–7338. [[CrossRef](#)] [[PubMed](#)]
20. Yi, L.; Ding, B.; Zhao, B.; Cheng, P.; Liao, D.Z.; Yan, S.P.; Jiang, Z.H. Novel triazole-bridged cadmium coordination polymers varying from zero-to three-dimensionality. *Inorg. Chem.* **2004**, *43*, 33–43. [[CrossRef](#)]
21. Aromí, G.; Barrios, L.A.; Roubeau, O.; Gamez, P. Triazoles and tetrazoles: Prime ligands to generate remarkable coordination materials. *Coord. Chem. Rev.* **2011**, *255*, 485–546. [[CrossRef](#)]
22. Kahn, O.; Martinez, C.J. Spin-Transition Polymers: From Molecular Materials Toward Memory Devices. *Science* **1998**, *279*, 44–48. [[CrossRef](#)]
23. Garcia, Y.; Bravic, G.; Gieck, C.; Chasseau, D.; Tremel, W.; Gütllich, P. Crystal Structure, Magnetic Properties, and ⁵⁷Fe Mössbauer Spectroscopy of the Two-Dimensional Coordination Polymers [M(1,2-bis(1,2,4-triazol-4-yl)ethane)₂(NCS)₂] (M^{II} = Fe, Co). *Inorg. Chem.* **2005**, *44*, 9723–9730. [[CrossRef](#)] [[PubMed](#)]
24. Grosjean, A.; Daro, N.; Kauffmann, B.; Kaiba, A.; Létard, J.F.; Guionneau, P. The 1-D polymeric structure of the [Fe(NH₂trz)₃](NO₃)₂·nH₂O (with n = 2) spin crossover compound proven by single crystal investigations. *Chem. Commun.* **2011**, *47*, 12382–12384. [[CrossRef](#)]
25. Ren, C.; Hou, L.; Liu, B.; Yang, G.P.; Wang, Y.Y.; Shi, Q.Z. Distinct structures of coordination polymers incorporating flexible triazole-based ligand: Topological diversities, crystal structures and property studies. *Dalton Trans.* **2011**, *40*, 793–804. [[CrossRef](#)]
26. Roubeau, O. Triazole-based one-dimensional spin-crossover coordination polymers. *Chem. A Eur. J.* **2012**, *18*, 15230–15244. [[CrossRef](#)]
27. Ouellette, W.; Yu, M.H.; O'Connor, C.J.; Hagrman, D.; Zubieta, J. Hydrothermal Chemistry of the Copper–Triazolate System: A Microporous Metal–Organic Framework Constructed from Magnetic {Cu₃(μ₃-OH)(triazolate)₃}²⁺ Building Blocks, and Related Materials. *Angew. Chem. Int. Ed.* **2006**, *45*, 3497–3500. [[CrossRef](#)]
28. Wang, Y.; Cheng, P.; Song, Y.; Liao, D.Z.; Yan, S.P. Self-Assembly and Anion-Exchange Properties of a Discrete Cage and 3D Coordination Networks Based on Cage Structures. *Chem. A Eur. J.* **2007**, *13*, 8131–8138. [[CrossRef](#)]
29. Naik, A.D.; Dîrtu, M.M.; Léonard, A.; Tinant, B.; Marchand-Brynaert, J.; Su, B.L.; Garcia, Y. Engineering three-dimensional chains of porous nanoballs from a 1, 2, 4-triazole-carboxylate supramolecular synthon. *Cryst. Growth Des.* **2010**, *10*, 1798–1807. [[CrossRef](#)]
30. Liu, W.; Shen, X.; Han, Y.; Liu, Z.; Dai, W.; Dutta, A.; Liu, J. Selective adsorption and removal of drug contaminants by using an extremely stable Cu (II)-based 3D metal-organic framework. *Chemosphere* **2019**, *215*, 524–531. [[CrossRef](#)]
31. Corella-Ochoa, M.N.; Tapia, J.B.; Rubin, H.N.; Lillo, V.; González-Cobos, J.; Núñez-Rico, J.L.; Galán-Mascarós, J.R. Homochiral metal–organic frameworks for enantioselective separations in liquid chromatography. *J. Am. Chem. Soc.* **2019**, *141*, 14306–14316. [[CrossRef](#)]
32. Kitchen, J.A.; Brooker, S. Spin crossover in iron (II) complexes of 3, 5-di (2-pyridyl)-1, 2, 4-triazoles and 3, 5-di (2-pyridyl)-1, 2, 4-triazolates. *Coord. Chem. Rev.* **2008**, *252*, 2072–2092. [[CrossRef](#)]
33. Garcia, Y.; Guionneau, P.; Bravic, G.; Chasseau, D.; Howard, A.K.J.; Kahn, O.; Ksenofontov, V.; Reiman, S.; Gütllich, P. Synthesis, Crystal Structure, Magnetic Properties and ⁵⁷Fe Mössbauer Spectroscopy of the New Trinuclear [Fe₃(4-(2'-hydroxyethyl)-1,2,4-triazole)₆(H₂O)₆](CF₃SO₃)₆ Spin Crossover Compound. *Eur. J. Inorg. Chem.* **2000**, *2000*, 1531–1538. [[CrossRef](#)]
34. Kitchen, J.A.; White, N.G.; Boyd, M.; Moubaraki, B.; Murray, K.S.; Boyd, P.D.W.; Brooker, S. Iron(II) Tris-[N⁴-substituted-3,5-di(2-pyridyl)-1,2,4-triazole] Complexes: Structural, Magnetic, NMR, and Density Functional Theory Studies. *Inorg. Chem.* **2009**, *48*, 6670–6679. [[CrossRef](#)] [[PubMed](#)]
35. Manrique-Juarez, M.D.; Mathieu, F.; Shalabaeva, V.; Cacheux, J.; Rat, S.; Nicu, L.; Leichlé, T.; Salmon, L.; Molnár, G.; Bousseksou, A. A Bistable Microelectromechanical System Actuated by Spin-Crossover Molecules. *Angew. Chem. Int. Ed.* **2017**, *56*, 8074–8190. [[CrossRef](#)] [[PubMed](#)]
36. Senthil Kumar, K.; Ruben, M. Emerging trends in spin crossover (SCO) based functional materials and devices. *Coord. Chem. Rev.* **2017**, *346*, 176–205. [[CrossRef](#)]
37. Molnár, G.; Rat, S.; Salmon, L.; Nicolazzi, W.; Bousseksou, A. Spin crossover nanomaterials: From fundamental concepts to devices. *Adv. Mater.* **2018**, *30*, 1703862. [[CrossRef](#)] [[PubMed](#)]
38. Depree, C.V.; Beckmann, U.; Heslop, K.; Brooker, S. Monomeric, trimeric and polymeric assemblies of dicopper (II) complexes of a triazolate-containing Schiff-base macrocycle. *Dalton Trans.* **2003**, *15*, 3071–3081. [[CrossRef](#)]
39. Klingele, M.H.; Moubaraki, B.; Cashion, J.D.; Murray, K.S.; Brooker, S. The first X-ray crystal structure determination of a dinuclear complex trapped in the [low spin–high spin] state:[Fe II 2 (PMAT) 2](BF 4) 4- DMF. *Chem. Commun.* **2005**, *8*, 987–989. [[CrossRef](#)]
40. Meng, Z.S.; Yun, L.; Zhang, W.X.; Hong, C.G.; Herchel, R.; Ou, Y.C.; Leng, J.D.; Peng, M.X.; Lin, Z.J.; Tong, M.L. Reactivity of 4-amino-3,5-bis(pyridin-2-yl)-1,2,4-triazole, structures and magnetic properties of polynuclear and polymeric Mn(II), Cu(II) and Cd(II) complexes. *Dalton Trans.* **2009**, *46*, 10284–10295. [[CrossRef](#)]
41. Ding, B.; Yi, L.; Wang, Y.; Cheng, P.; Liao, D.Z.; Yan, S.P.; Jiang, Z.H.; Song, H.B.; Wang, H.G. Synthesis of a series of 4-pyridyl-1, 2, 4-triazole-containing cadmium (II) luminescent complexes. *Dalton Trans.* **2006**, *5*, 665–675. [[CrossRef](#)] [[PubMed](#)]
42. Li, W.; Li, M.X.; Shao, M.; Wang, Z.X.; Liu, H.J. Ferromagnetic and mixed-valence copper coordination polymers assembled by polycarboxylates and 2, 6-bis (1, 2, 4-triazolyl) pyridine. *Inorg. Chem. Commun.* **2008**, *11*, 954–957. [[CrossRef](#)]
43. Tahli, A.; Maclaren, J.K.; Boldog, I.; Janiak, C. Synthesis and crystal structure determination of 0D-, 1D-and 3D-metal compounds of 4-(pyrid-4-yl)-1, 2, 4-triazole with zinc (II) and cadmium (II). *Inorg. Chim. Acta* **2011**, *374*, 506–513. [[CrossRef](#)]

44. Garcia, Y.; Kahn, O.; Rabardel, L.; Chansou, B.; Salmon, L.; Tuchagues, J.P. Two-Step Spin Conversion for the Three-Dimensional Compound Tris (4, 4'-bis-1, 2, 4-triazole) iron (II) Diperchlorate. *Inorg. Chem.* **1999**, *38*, 4663–4670. [[CrossRef](#)]
45. Drabent, K.; Ciunik, Z.; Ozarowski, A. X-ray crystal structures, electron paramagnetic resonance, and magnetic studies on strongly antiferromagnetically coupled mixed μ -hydroxide- μ -N 1, N 2-triazole-bridged one dimensional linear chain copper (II) complexes. *Inorg. Chem.* **2008**, *47*, 3358–3365. [[CrossRef](#)] [[PubMed](#)]
46. Boland, Y.; Tinant, B.; Safin, D.A.; Marchand-Brynaert, J.; Clérac, R.; Garcia, Y. A metal–organic framework made of an asymmetric 1, 2, 4-triazole and tetrazole ligand. *CrystEngComm* **2012**, *14*, 8153–8155. [[CrossRef](#)]
47. Roubeau, O.; Alcazar Gomez, J.M.; Balskus, E.; Kolnaar, J.J.A.; Haasnoot, J.G.; Reedijk, J. Spin-transition behaviour in chains of FeII bridged by 4-substituted 1, 2, 4-triazoles carrying alkyl tails. *N. J. Chem.* **2001**, *25*, 144–150. [[CrossRef](#)]
48. Kahn, O.; Kröber, J.; Jay, C. Spin Transition Molecular Materials for displays and data recording. *Adv. Mater.* **1992**, *4*, 718–728. [[CrossRef](#)]
49. Kröber, J.; Codjovi, E.; Kahn, O.; Grolière, F.; Jay, C. A Spin Transition System with a Thermal Hysteresis at Room Temperature. *J. Am. Chem. Soc.* **1993**, *115*, 9810–9811. [[CrossRef](#)]
50. Pittala, N.; Thétiot, F.; Charles, C.; Triki, S.; Boukheddaden, K.; Chastanet, G.; Marchivie, M. An unprecedented trinuclear Fe II triazole-based complex exhibiting a concerted and complete sharp spin transition above room temperature. *Chem. Comm.* **2017**, *53*, 8356–8359. [[CrossRef](#)]
51. Kolnaar, J.J.A.; van Dijk, G.; Kooijman, H.; Spek, A.L.; Ksenofontov, V.G.; Gütllich, P.; Haasnoot, J.G.; Reedijk, J. Synthesis, Structure, Magnetic Behavior, and Mössbauer Spectroscopy of Two New Iron(II) Spin-Transition Compounds with the Ligand 4- Isopropyl-1,2,4-triazole. X-ray Structure of [Fe₃(4-isopropyl-1,2,4- triazole)₆(H₂O)₆](tosylate)₆·2H₂O. *Inorg. Chem.* **2002**, *36*, 2433–2440. [[CrossRef](#)] [[PubMed](#)]
52. Gómez, V.; Sáenz de Pipaón, C.; Maldonado-Illescas, P.; Waerenborgh, J.C.; Martin, E.; Benet-Buchholz, J.; Galán-Mascarós, J.R. Easy Excited-State Trapping and Record High T_{TIESST} in a Spin-Crossover Polyanionic Fe^{II} Trimer. *J. Am. Chem. Soc.* **2015**, *137*, 11924–11927. [[CrossRef](#)] [[PubMed](#)]
53. See, R.F.; Kruse, R.A.; Strub, W.M. Metal–ligand bond distances in first-row transition metal coordination compounds: Coordination number, oxidation state, and specific ligand effects. *Inorg. Chem.* **1998**, *37*, 5369–5375. [[CrossRef](#)]
54. Lloret, F.; Julve, M.; Cano, J.; Ruiz-García, R.; Pardo, E. Magnetic properties of six-coordinated high-spin cobalt (II) complexes: Theoretical background and its application. *Inorg. Chim. Acta* **2008**, *361*, 3432–3445. [[CrossRef](#)]
55. Yang, J.; Ma, Y.S.; Tang, X.Y.; Shen, L.; Yuan, R.X.; Zhu, D.R.J. Syntheses, crystal structures, and spectral characterization of two new Cu (II) and Co (II) complexes with an asymmetrical substituted triaryltriazole. *Coord. Chem.* **2011**, *64*, 3980–3991.
56. Borrás-Almenar, J.J.; Clemente-Juan, J.M.; Coronado, E.; Tsukerblat, B.S. High-nuclearity magnetic clusters: Generalized spin Hamiltonian and its use for the calculation of the energy levels, bulk magnetic properties, and inelastic neutron scattering spectra. *Inorg. Chem.* **1999**, *38*, 6081–6088. [[CrossRef](#)]
57. Ramos, E.; Roman, J.E.; Cardona-Serra, S.; Clemente-Juan, J.M. Parallel implementation of the MAGPACK package for the analysis of high-nuclearity spin clusters. *Comput. Phys. Commun.* **2010**, *181*, 1929–1940. [[CrossRef](#)]
58. Vos, G.; Haasnoot, J.G.; Verschoor, G.C.; Reedijk, J.; Schaminee, P.E.L. Linear trinuclear coordination compounds with 4-ethyl-1, 2, 4-triazole. Structure and magnetic properties. *Inorg. Chim. Acta* **1985**, *105*, 31–39. [[CrossRef](#)]
59. Baca, S.G.; Sevryugina, Y.; Clérac, R.; Malaestean, I.; Gerbeleu, N.; Petrukhina, M.A. Linear trinuclear manganese (II) complexes: Crystal structures and magnetic properties. *Inorg. Chem. Commun.* **2005**, *8*, 474–478. [[CrossRef](#)]
60. Ding, B.; Yi, L.; Shen, W.Z.; Cheng, P.; Liao, D.Z.; Yan, S.P.; Jiang, Z.H. Synthesis, crystal structure and magnetic properties of N1, N2-bridged polynuclear Ni (II) complexes. *J. Mol. Struct.* **2006**, *784*, 138–143. [[CrossRef](#)]
61. Siddiqui, K.A.; Mehrotra, G.K.; Mrozinski, J.; Butcher, R.J. Anion assisted self-assembly of a Ni (II) complex into metallo-supramolecular network involving H-bonded synthons as nodes. *J. Mol. Struct.* **2010**, *964*, 18–26. [[CrossRef](#)]
62. Tong, Y.Z.; Wang, Q.L.; Si, M.; Qi, J.; Yan, S.P.; Yang, G.M.; Cheng, P.; Liao, D.Z. Crystal structure, spectroscopy and magnetism of trinuclear nickel (II), cobalt (II) complexes and their solid solution. *Polyhedron* **2011**, *30*, 3151–3157. [[CrossRef](#)]
63. Aznar, E.; Ferrer, S.; Borrás, J.; Lloret, F.; Liu-González, M.; Rodríguez-Prieto, H.; García-Granda, S. Coordinative Versatility of Guanazole [3,5-Diamino-1,2,4-triazole]: Synthesis, Crystal Structure, EPR, and Magnetic Properties of a Dinuclear and a Linear Trinuclear Copper(II) Complex Containing Small Bridges and Triazole Ligands. *Eur. J. Inorg. Chem.* **2006**, 5115–5125. [[CrossRef](#)]
64. Koomen-Van Oudenniel, W.M.E.; De Graaff, R.A.G.; Haasnoot, J.G.; Prins, R.; Reedijk, J. Magnetic and spectroscopic properties of copper (II) compounds with alkyl-disubstituted triazoles. X-ray structure of bis [μ -4-amino-3, 5-bis (aminomethyl)-1, 2, 4-triazole-N', N1, N2, N''] bis [aquabromocopper (II) dibromide-2-water-methanol. *Inorg. Chem.* **1989**, *28*, 1128–1133. [[CrossRef](#)]
65. Slangen, P.M.; van Koningsbruggen, P.J.; Haasnoot, J.G.; Jansen, J.; Gorter, S.; Reedijk, J.; Kooijman, H.; Smeets, W.J.J.; Spek, A.L. Synthesis, characterization, crystal structures and magnetic properties of di-and polynuclear bis (μ -3-pyridin-2-yl-1, 2, 4-triazolato) copper (II) compounds containing N-methylimidazole, pyrazole or 4, 4'-bipyridine as co-ligands. *Inorg. Chim. Acta* **1993**, *212*, 289–301. [[CrossRef](#)]
66. Garcia, Y.; van Koningsbruggen, P.J.; Bravic, G.; Guionneau, P.; Chasseau, D.; Cascarano, G.L.; Moscovici, J.; Lambert, K.; Michalowicz, A.; Kahn, O. Synthesis, Crystal Structure, EXAFS, and Magnetic Properties of catena-Poly [μ -tris (4-(2-hydroxyethyl)-1, 2, 4-triazole-N 1, N 2) copper (II)] Diperchlorate Trihydrate: Relevance with the Structure of the Iron (II) 1, 2, 4-Triazole Spin Transition Molecular Materials. *Inorg. Chem.* **1997**, *36*, 6357–6365.

67. Ding, B.; Huang, Y.Q.; Liu, Y.Y.; Shi, W.; Cheng, P. Synthesis, structure and magnetic properties of a novel 1D coordination polymer $\{[\text{Cu}_2(\text{amtrz})_4(1, 1-\mu\text{-NCS})_2](\text{ClO}_4)_2 \cdot \text{H}_2\text{O}\}_n$. *Inorg. Chem. Commun.* **2007**, *10*, 7–10. [[CrossRef](#)]
68. Dumestre, F.; Soula, B.; Galibert, A.M.; Fabre, P.L.; Bernardinelli, G.; Donnadiou, B.; Castan, P.J. Synthesis and characterization of cobalt (II) complexes of croconate and dicyanomethylene-substituted derivatives. *Chem. Soc. Dalton Trans.* **1998**, *24*, 4131–4138. [[CrossRef](#)]
69. Woolf, A.A. Tetrahedral Geometry Made Simple. *J. Chem. Educ.* **1995**, *72*, 19. [[CrossRef](#)]
70. Oka, Y.; Inoue, K. Structures and magnetic properties of a new cobalt (II) linear trimer with phenylcinnamic acid. *Chem. Lett.* **2004**, *33*, 402. [[CrossRef](#)]
71. Coelho, A.A.; Evans, J.; Evans, I.; Kern, A.; Parsons, S. The TOPAS symbolic computation system. *Powder Diffr.* **2011**, *26*, S22–S25. [[CrossRef](#)]
72. Coronado, E.; Day, P. Magnetic molecular conductors. *Chem. Rev.* **2004**, *104*, 5419–5448. [[CrossRef](#)] [[PubMed](#)]
73. Bujak, P.; Kulszewicz-Bajer, I.; Zagorska, M.; Maurel, V.; Wielgus, I.; Pron, A. Polymers for electronics and spintronics. *Chem. Soc. Rev.* **2013**, *42*, 8895–8999. [[CrossRef](#)] [[PubMed](#)]